

Synergistic Effect of Chemotherapy and Magnetomechanical Actuation of Fe-Cr-Nb-B Magnetic Particles on Cancer Cells

Cristina Staviř, Anca Emanuela Minuti,* Dumitru Daniel Herea, Luminiřa Lăbușcă, Daniel Gherca, Nicoleta Lupu, and Horia Chiriac



Cite This: *ACS Omega* 2024, 9, 30518–30533



Read Online

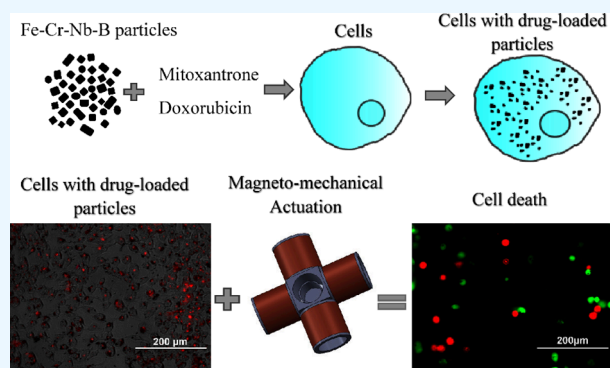
ACCESS |

Metrics & More

Article Recommendations

Supporting Information

ABSTRACT: The present study is aimed at developing an innovative method for efficient cancer cell destruction by exploiting the magnetomechanical actuation (MMA) of Fe-Cr-Nb-B magnetic particles (MPs), which are loaded with clinically approved chemotherapeutic drugs. To achieve this objective, $\text{Fe}_{68.2}\text{Cr}_{11.5}\text{Nb}_{0.3}\text{B}_{20}$ magnetic nanoparticles were produced by mechanically grinding amorphous ribbon precursors with the same composition. These nanoparticles display high anisotropy, a parallelepipedic shape with an amorphous structure, and a ferromagnetic behavior. MPs were loaded with the antitumoral drugs mitoxantrone (MTX) or doxorubicin (DOX). In our study, we used adipose-derived mesenchymal stem cells and human osteosarcoma cells to test drug-loaded MPs for their biocompatibility, cytotoxicity, and cellular internalization. Further tests involved exposing cells to magnetomechanical actuation and simultaneous MPs-targeted chemotherapy followed by cell viability/death assays, such as MTT and LDH, and live/dead cell staining. Results demonstrate that cancer cell death was induced by the synergistic action of chemotherapeutic drugs and magnetomechanical actuation. The nanoparticle vehicles helped overcome drug resistance, decreasing the high dose of drugs used in conventional therapies as well as the time intervals needed for MMA to affect cancer cell viability. The proposed approach highlights the possibility of using a new, targeted, and effective cancer treatment with very few side effects.



1. INTRODUCTION

Magnetic nanoparticles (MPs) have acquired considerable attention in biomedical research due to their potential applications. Their adjustable properties, including size, shape, composition, surface chemistry, and magnetic characteristics, render them versatile tools for various purposes. A notable advantage of these nanomaterials lies in their responsiveness to both static and dynamic magnetic fields. The gained momentum of magnetic particles within a magnetic field, particularly in dynamic magnetic fields, has been explored for cancer diagnosis and treatment.¹ Magnetomechanical actuation (MMA) implies an external rotating magnetic field aimed to induce the mechanical movement of magnetic nanoparticles according to applied field directions. Consequently, the resulting motions generate mechanical forces and magnetic torque in MPs capable of manipulating biomolecules or cellular structures situated nearby.² To enhance magnetic torque, it is considered necessary for nanoparticles to possess increased magnetic anisotropy and saturation magnetization.³ This rotational capability holds significant implications in the realm of remote apoptosis induction. Upon encountering cellular membranes, the nanoparticles begin the process of internalization, managing to

traverse the cell membrane. Subsequent internalization leads to the binding of the MPs to the lysosomal membrane. Subjecting the samples to MMA induces the rotational movement of the MPs, consequently engendering shear forces that disrupt the integrity of the lysosomal membrane. Consequently, lysosomal contents are released into the cytoplasm, thereby precipitating a decline in its pH and eventual initiation of apoptosis.⁴

In the context of cancer treatment, iron oxide particles and alloys of Ni, Co, and NiFe have been utilized for magneto-mechanical actuation.⁵ Our group introduced $\text{Fe}_{68.2}\text{Cr}_{11.5}\text{Nb}_{0.3}\text{B}_{20}$ nanoparticles produced by mechanical grinding in a high-ball energy mill of amorphous ribbon precursors with the same composition, previously obtained by rapid melt quenching. These MPs exhibit high anisotropy, parallelepipedic shape (with sizes ranging from 10 to 200 nm), amorphous structure, and ferromagnetic behavior and have

Received: March 7, 2024

Revised: June 12, 2024

Accepted: June 14, 2024

Published: July 1, 2024



shown promising results in reducing cancer cell viability under magnetomechanical actuation.⁶

The objective of this study is to develop a method for efficient cancer cell destruction through a synergistic approach, combining magnetomechanical actuation with clinically used antitumoral drugs. For our study, we used human osteosarcoma cells (HOS) as cancer cell representatives and adipose-derived mesenchymal stem cells (ADSCs) as nontumoral representatives and possible carriers for MPs. ADSCs have gained attention in recent years for their potential use in the treatment of some diseases such as musculoskeletal disorders, osteoarthritis, autoimmune diseases, heart diseases, diabetes, obesity, wound-healing, and neurologic and nephrogenic diseases.⁷ ADSCs present many advantages such as availability, high *in vitro* production, low-pain minimally invasive harvesting techniques, potential to differentiate in multiple lineage cells, and immunomodulatory properties, which make them suitable carriers for magnetic nanoparticles.

The obtained Fe_{68.2}Cr_{11.5}Nb_{0.3}B₂₀ magnetic nanoparticles are used for the drug loading of chemotherapeutics: mitoxantrone (MTX) or doxorubicin (DOX). These drugs are approved by the FDA and used in clinical practice for several types of cancer.^{8,9} The drug-loaded Fe-Cr-Nb-B particles enter the cell body and might function as a nanovehicle for drug delivery, facilitating the bypass multidrug resistance mechanism of cancer cells. Magnetomechanical actuation of these particles leads to cell membrane rupture followed by cell death. The biocompatibility of nanoparticles was evaluated by using the MTT assay, and drug-loading with mitoxantrone or doxorubicin was confirmed by FTIR analysis. Drug loading efficiency (DL, %), drug encapsulation efficiency (EE, %), and *in vitro* drug release were determined through spectrophotometric measurements. A ferrozine assay was utilized to evaluate the internalization of nanoparticles into ADSCs and HOS cells. The cytotoxicity of drug-loaded MPs was evaluated by an MTT assay and cell nucleus DAPI staining. The study further involved exposing cells to MMA and evaluating cell death through MTT, LDH assays, and live/dead cell staining in both cell lines. Additionally, ADSCs were tested for their potential use as MP carriers. The drug-loaded MPs in ADSCs were transferred to HOS cell cultures and exposed to MMA. Further, HOS internalized the released MPs and were actuated in a magnetic field for cancer cell destruction with results assessed through MTT and LDH assays. In all cases presented above, the cancer cell death was triggered by two combined factors: chemotherapeutic drugs and magnetomechanical actuation. Nanoparticle vehicles helped to overcome drug resistance, decreasing conventional high doses of drugs used in systemic administration and time needed for MMA exposure.

2. METHODS

2.1. Magnetic Nanoparticle Preparation. Magnetic nanoparticles Fe_{68.2}Cr_{11.5}Nb_{0.3}B₂₀ were prepared by a ball-milling process from amorphous rapid quenched melt-spun ribbons with the same composition. Cr-containing magnetic alloys were prepared using high-purity raw materials (Fe 68.2%, Cr 11.5%, Nb 0.3%, and B 20%) that were degassed by vacuum melting before being alloyed. The alloys were melted using induction, remelted several times, and then turned into ribbons to avoid any inhomogeneity. Amorphous ribbons were melt spun by rapidly cooling the Fe-Cr-Nb-B alloy in a tubular quartz crucible. The ribbons were then thermally treated in a vacuum at 400 °C to make them more fragile for mechanical

grinding. The strips were mechanically milled using a Fritsch Vibratory Ball Mill (Pulverisette 7 Premium Model) with two grinding chambers and oleic acid as a surfactant. The ball-to-powder ratio (BPR) was 50:1, the rotation speed of the chambers was 550 rpm, and the degree of filling was approximately 50%. Grinding was carried out in a humid environment using high-purity argon. Powders were obtained after 360 h of grinding. Finally, the obtained particles were washed in heptane in an ultrasound bath, dried in a vacuum oven at 700 °C, and kept in a vacuum chamber.¹⁰

The unique composition of Fe-Cr-Nb-B magnetic particles is achieved through precise control of the alloying process, which is under international patent. This allows for tailoring the composition and properties to meet specific application requirements. Furthermore, coating the nanoparticles with oleic acid is crucial for achieving the desired particle size, dispersion, and stability.

2.2. Ferrofluid Preparation. A ferrofluid was prepared from Fe-Cr-Nb-B nanoparticles for better dispersibility and biocompatibility. MPs were washed three times with NaOH 5% to remove the excess oleic acid from the nanoparticles' surface and five times with ultrapure water in an ultrasonic bath to reach a pH of 7. The ferrofluid was made using 1 mL of 94 mg/mL calcium gluconate solution by ultrasonication with an ultrasonic probe for 30 min at 80 °C. The ferrofluid was sterilized at 121 °C for 30 min using an autoclave.¹¹

2.3. Nanoparticle Drug Loading. **2.3.1. Drug Loading and Spectrophotometric Quantification.** Magnetic nanoparticles were loaded with either mitoxantrone or doxorubicin in an aqueous solution of these chemotherapeutic drugs. Solutions of established concentration (100 µg/mL) were prepared by dissolving mitoxantrone hydrochloride (Merck) and doxorubicin hydrochloride (Merck) in ultrapure water. For sterile conditions, drug solutions were sterilized by using a sterile syringe filter of 0.22 µm. Loading of Fe-Cr-Nb-B nanoparticles was achieved by adding the nanoparticles to MTX/DOX solutions in 15 mL centrifuge tubes that were placed on a rotative shaker for 24 h. After the binding reaction, nanoparticles were centrifuged at 4500g for 10 min (Hettich Benchtop centrifuge ROTANTA 460), and the supernatant was collected and analyzed for the unloaded (free) amounts of MTX/DOX. The loaded amounts of MTX and DOX were calculated by subtracting the unloaded amounts from the total amount. The concentration of MTX and DOX was determined using a spectrophotometric method by monitoring the absorption of MTX at 610 nm and DOX at 480 nm with a Multi-Mode Microplate Reader Synergy HTX. Drug loading efficiency (DL, %) and drug encapsulation efficiency (EE, %) were calculated according to the following equations:¹²

$$DL (\%) = \frac{\text{total weight of the drug (Wt)}}{\text{total weight of nanoparticles}} \times 100$$

$$= \frac{\text{free weight of the drug in supernatant (Wfree)}}{\text{total weight of nanoparticles}} \times 100$$

$$EE (\%) = \frac{\text{total weight of the drug (Wt)}}{\text{total weight of the drug (Wt)}} \times 100$$

$$= \frac{\text{free weight of the drug in supernatant (Wfree)}}{\text{total weight of the drug (Wt)}} \times 100$$

Fourier Transform Infrared Spectroscopy (FTIR) Analysis. FTIR analysis reveals the bonding between Fe-Cr-Nb-B nanoparticles and active drug compounds, namely, mitoxan-

trone and doxorubicin. For FTIR analysis, a spectrophotometer (Jasco, FT/IR-6100 model) was used, and infrared spectra of magnetic nanoparticles by the KBr pelletizing technique were recorded in the 4000–400 cm^{-1} region at a resolution of 4 cm^{-1} .

2.4. In Vitro Drug Release of MTX or DOX from Fe-Cr-Nb-B Particles. Drug-releasing profiles for both mitoxantrone and doxorubicin were investigated for quantifying the delivered drug over a certain amount of time. The release profiles of MTX and DOX from the magnetic nanoparticles were determined according to the adapted dialysis bag method. In brief, 5 mg of Fe-Cr-Nb-B nanoparticles loaded with MTX/DOX was distributed in 1 mL of culture medium without phenol red and placed in dialysis bags made of dialysis membranes (MWCO: 14,000) tied from both sides. The bags were dialyzed against 4 mL of culture medium at a pH of 7.4 (mimicking physiological pH) and acidic pH 6.0 and 4.5 under shaking at 37 °C. At specific time intervals, aliquots of 0.2 mL were withdrawn and replaced with an equal volume of fresh culture medium. The samples were evaluated in a 96-well plate, in duplicate for each value, and read with the Multi-Mode Microplate Reader Synergy HTX via UV–vis spectrometry at 610 nm for MTX and 480 nm for DOX. The cumulative drug release was calculated based on the standard curves for MTX and DOX obtained in the culture medium using the following equation. The *in vitro* release experiments were performed in triplicate to confirm their reproducibility.¹³

$$\text{Cumulative release (\%)} = \frac{A_n + \frac{v}{vt} \sum_{k=0}^{n-1} A_k}{A_c} \times 100$$

where v = volume of the release medium extracted at each time point (i.e., 0.2 mL); vt = total volume of release medium (i.e., 5 mL); A_n = absorbance of the samples at time point n ; A_k = absorbance of the samples at time point k , where $k \in [0, n - 1]$; A_c = absorbance of controls (i.e., MTX and DOX in the culture medium matching the concentration of the drug adsorbed by Fe-Cr-Nb-B nanoparticles), and n ($\neq 0$) is the time point for sample collection.

The experimental data were evaluated using five distinct models of drug release kinetics. The data from the zero-order model were represented by plotting the cumulative percentage of drug release against time. For the first-order model, the data were plotted as the logarithm of the cumulative percentage of drug release versus time. In the case of the Korsmeyer–Peppas model, the data were plotted as the logarithm of the cumulative percentage of drug release against the logarithm of time. Meanwhile, the Higuchi model data were depicted by plotting the cumulative percentage of drug release against the square root of time. Lastly, the Hixson–Crowell model data were represented by plotting the cube root of drug percentage remaining on nanoparticles against time.¹⁴

2.5. Cell Culture, Cell Viability, and Cytotoxicity.

Adipose-derived stem cells (ADSCs) and human osteosarcoma cells (HOS) were cultured using complete culture media (DMEM, 10% FBS, 1% antibiotic/antimycotic), seeded in 96-well plates at 10^4 cells/well and 37 °C at 5% CO_2 , and incubated until 90% confluency.

2.5.1. MTT Viability Assay. The MTT (3-(4,5-dimethylthiazolyl-2)-2,5-diphenyltetrazolium bromide) assay was used for determining the viability of cells after a specific treatment or interactions compared with control cells. Adipose-derived stem cells (ADSCs) and human osteosarcoma cells (HOS)

were cultured using complete culture media (DMEM, 10% FBS, 1% antibiotic/antimycotic), seeded in 96-well plates at 10^4 cells/well and 37 °C at 5% CO_2 , and incubated until 90% confluency. After reaching cell confluency, MPs and MPs loaded with MTX/DOX were added to fresh culture media. Cell viability was determined using the MTT assay (Thermo-Fisher Scientific) according to the supplier's instructions, which are based on quantifying cell metabolic activity by reducing tetrazolium salt in intracellular formazan that is solubilized with DMSO and further quantified by spectrophotometric methods.

The cell viability (%) is calculated using the following equation:¹⁵

$$\text{CV (\%)} = 100 \times \frac{A_{\text{Ferrofluid}} - A_{\text{Blank}}}{A_{\text{Control}} - A_{\text{Blank}}}$$

CV (%) is the cell viability, and A_b represents the measured absorbance of (a) cells with ferrofluid ($A_{\text{Ferrofluid}}$), (b) control cells (A_{Control}), and (c) cell culture media in the well (A_{Blank}). The absorbance was measured at 570 nm with the Multi-Mode Microplate Reader Synergy HTX spectrophotometer.

The MTT data were used for determination of the IC_{50} (half-maximal inhibitory concentration). Data of cell viability were plotted against drug concentrations, and a linear regression fitting was used. The linear fitting graphs for each sample of cells for determination of IC_{50} are presented in Figures S9 and S10.

2.5.2. Lactate Dehydrogenase (LDH) Cytotoxicity Assay. A CyQUANT LDH Cytotoxicity Assay Kit (Invitrogen) was used for cytotoxicity assay following manufacturer instructions. The lactate dehydrogenase (LDH) assay is a colorimetric formazan-based method used to identify cell cytotoxicity by measuring the released LDH cytosolic enzyme after cell membrane rupture. For assessing 96-well plates with HOS and ADSCs at 90% confluency were loaded with MPs or drug-loaded MPs for 24 h. After this time, the same cells were subjected to MMA. LDH release was assessed after 12 h. Each sample had five wells ($n = 3$), including spontaneous LDH activity controls and maximum LDH activity controls. Maximum LDH activity controls were lysed with 10 μL of 10 \times lysis buffer, and for spontaneous LDH activity, 10 μL of water was added to each well. The plate was incubated at 37 °C for 45 min. Fifty microliters of culture media from each well was transferred into a new plate, 50 μL of reaction mixture from the assay kit was added, and the mixture was incubated for 30 min protected from light at room temperature. Further 50 μL of stop solution was added, and the absorbance was measured at 490 and 680 nm using a microplate spectrophotometric reader. The 680 nm absorbance value was the background signal from the instrument and was subtracted from the 490 nm value. Cytotoxicity was calculated following the equation below:

$$\begin{aligned} \text{\%Cytotoxicity} &= \frac{\text{sample LDH activity} - \text{spontaneous LDH activity}}{\text{maximum LDH activity} - \text{spontaneous LDH activity}} \\ &\times 100 \end{aligned}$$

2.6. Cellular Internalization of MPs and Drug-Loaded MPs. **2.6.1. Ferrozine Assay.** To study the cellular uptake of Fe-Cr-Nb-B with or without MTX/DOX, ADSCs and HOS cells were grown in 24-well culture plates to reach a confluent

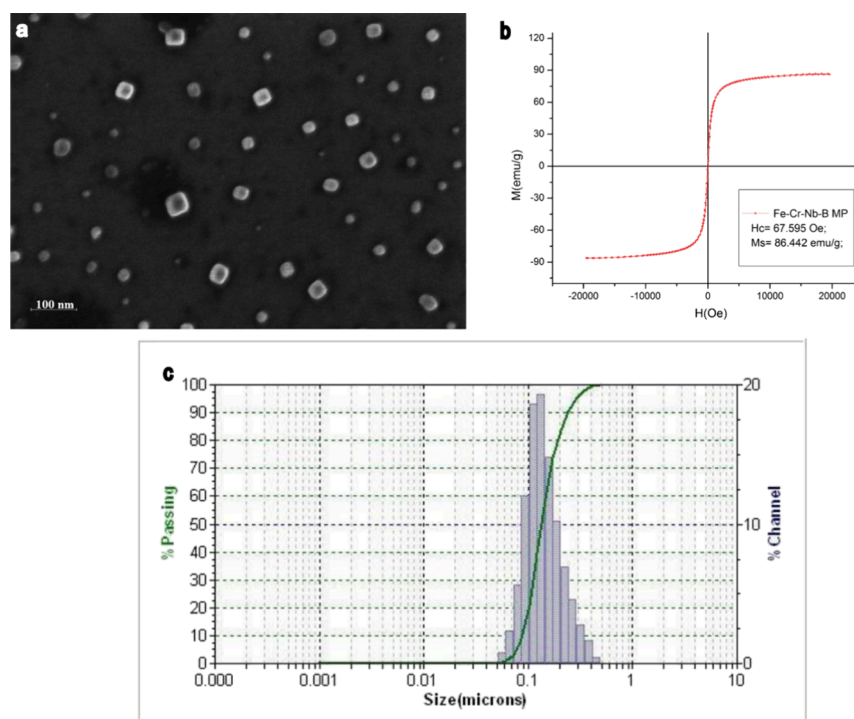


Figure 1. Fe-Cr-Nb-B magnetic particle properties. (a) HR-SEM image of particles showing the size and size distribution of magnetic particles. (b) VSM-hysteresis loop of Fe-Cr-Nb-B particles. (c) Fe-Cr-Nb-B diameter distribution measurements obtained by DLS.

monolayer. Afterward, a cell culture medium containing MP/MP-MTX/MP-DOX was added to the cell culture wells and coincubated for 24 h. To identify if there are differences in cellular uptake at different drug quantity loadings, tests were performed with 1 mg/mL of MPs and MPs coupled with 1 and 10 μg of MTX/DOX per 1 mg of nanoparticles. After 24 h, the culture medium was removed, and the samples were washed twice with ice-cold PBS to remove nonadherent nanoparticles. After completely removing the PBS, the cells were frozen, and the dishes were stored at $-20\text{ }^{\circ}\text{C}$. Cells were lysed with 200 μL of 50 mM NaOH for 2 h on a shaker. Aliquots (100 μL) of cell lysates were placed in Eppendorf tubes and mixed with 100 μL of 10 mM HCl and 100 μL of the iron-releasing reagent (freshly mixed solution of equal volumes of 1.4 M HCl and 4.5% (w/v) KMnO_4 in H_2O). The mixtures were incubated for 2 h at $60\text{ }^{\circ}\text{C}$. After the mixtures had cooled to room temperature, 30 μL of the iron-detection reagent (6.5 mM ferrozine, 6.5 mM neocuproine, 2.5 M ammonium acetate, and 1 M ascorbic acid dissolved in water) was added to each tube. After 30 min, 280 μL of the solution in each tube was transferred into a 96-well plate, and the absorbance was measured at 550 nm by a Synergy HTX plate reader. The concentration of MPs was quantified based on an iron standard solution. A calibration curve was made using FeCl_3 standards (0–300 μM) in 10 mM HCl to allow the calculation of iron content per sample.¹⁶

2.6.2. DAPI (4',6-Diamidino-2-phenylindole) Staining. DAPI, a blue-fluorescent dye for DNA in cell nuclei, is used for microscopy visualization of cellular nuclei. For identifying the iron quantity intake per cell, an indirect method of nucleus cell counting was utilized. Cells were washed with PBS twice and fixed with 70% ethanol for 20 min. After ethanol was removed, DAPI (ThermoFisher Scientific) staining was added to cells and incubated at room temperature for 5 min. Samples were washed with PBS to remove DAPI excess and assessed

with an EVOS inverted light microscope DAPI filter. An average of five captions was taken for each well, and nucleus counting was processed by the ImageJ software.

The same DAPI staining protocol was used for nucleus observation. After DAPI staining, cells were imaged with an EVOS inverted light microscope in a DAPI fluorescence filter at 40 \times magnification.

2.7. Magnetomechanical Actuation. The magneto-mechanical actuation of Fe-Cr-Nb-B particles involves subjecting them to a rotating magnetic field at a low frequency. The experimental system devised in our laboratory comprises an assembly of four coils arranged in a cross configuration.¹⁷ These coils can generate a uniform rotating magnetic field with values of up to 200 Oe within a space of approximately 20 cm^3 . Two waveforms pass through the coil system, each phase-shifted by 90° . This configuration aligns with the orthogonal layout of the coil system, enabling the magnetic field to undergo rotation at the frequency of the waveforms, spanning from a few mHz to kHz. Cell culture plates were situated within the coil system's uniform magnetic field area and subjected to the rotating magnetic field, leading to the movement of magnetic particles followed by cell destruction and subsequent cell death.

2.8. MPs-Loaded ADSC Transfer onto HOS Culture. ADSCs were loaded with MP-MTX and MP-DOX for nanoparticle transportation onto the HOS culture. ADSCs were seeded in 96-well plates containing 10^4 cells/well in complete culture media and grown until 90% confluency. Further fresh culture media with 1 mg/mL MPs either loaded with MTX/DOX or nonloaded were added to cell cultures. After internalization of MPs for 24 h, ADSCs were washed with PBS, trypsinized, resuspended in complete culture media, and added onto HOS at confluency. After 2 h of coincubation, samples were subjected to magnetomechanical actuation for 30 min to release the MPs from ADSC carriers in HOS culture.

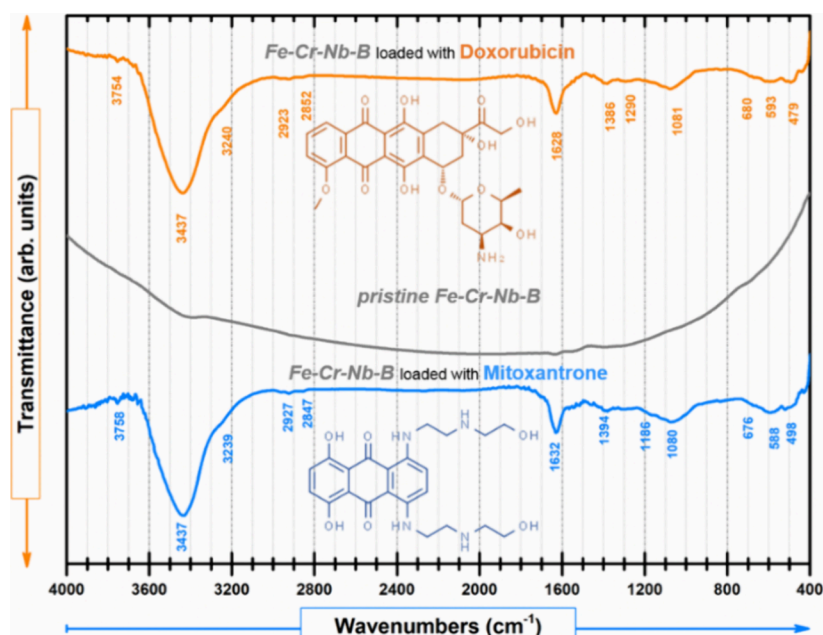


Figure 2. Comparative FTIR spectra of Fe-Cr-Nb-B magnetic nanoparticles loaded with mitoxantrone (MP-MTX) and doxorubicin (MP-DOX) versus pristine Fe-Cr-Nb-B magnetic nanoparticles. Molecular structures of mitoxantrone and doxorubicin are provided as insets, illustrating their chemical frameworks and highlighting the functional groups responsible for interactions with Fe-Cr-Nb-B MPs.

The plates were further incubated for 24 h and exposed to a new session of MMA to destroy those already loaded with MP HOS.

2.9. Live/Dead Staining. Live/dead fluorescent staining (Invitrogen) is used for identifying live cells colored green and dead cells colored red. HOS and ADSCs were cultured in six-well plates until 90% confluency. Twenty-four hours after adding MPs or drug-loaded MPs, cells were subjected to MMA as described earlier. After another 12 h, cells were washed twice with cell culture-grade PBS. A solution of 2 μM calcein AM and 4 μM EthD-1 was made, and 0.5 mL was added in each well. Cells were incubated for 45 min in the absence of light at room temperature. Cells were washed with PBS and assessed with an EVOS inverted light microscope using fluorescence filters (RFP for dead cells/GFP for live cells) also in bright field and overlay (merged images of bright field, RFP, and GFP).

2.10. Statistical Analysis. Statistical analysis was performed using the OriginPro 8 software. The comparison between groups was assessed by one-way ANOVA followed by Bonferroni correction. Significant statistical difference between groups was considered for $p < 0.05$. All significant different groups were marked on the images with * for $p < 0.05$.

3. RESULTS AND DISCUSSION

3.1. Fe-Cr-Nb-B Magnetic Nanoparticle Preparation and Characterization. Amorphous ribbons with the composition $\text{Fe}_{68.2}\text{Cr}_{11.5}\text{Nb}_{0.3}\text{B}_{20}$ were prepared through rapid quenching from the melt into a rotating water layer. Because of the amorphous state, the magnetic ribbons present specific magnetic properties such as elevated magnetic permeability, high saturation magnetization achieved at low magnetic fields, and controlled Curie temperature. Following heat treatment for embrittlement, the amorphous ribbons undergo a mechanical grinding process in a high-energy mill until particles reach nanosize dimensions. During the milling process, the particles retain their initial amorphous state.

Through this technique, magnetic particles with dimensions ranging from 10 to 200 nm are obtained, exhibiting a parallelepipedic shape, as depicted in Figure 1a obtained using an HR-SEM. DLS (dynamic light scattering) measurements shown in Figure 1c revealed the size range of Fe-Cr-Nb-B magnetic particles to be between 50 and 500 nm. DLS hydrodynamic diameter results have higher values due to the water shell surrounding particles leading to larger sizes compared to HR-SEM images.

These particles, with a saturation magnetization of 86 emu/g, demonstrate a rapid increase in magnetization with the magnetic field starting from low values. The results were obtained using a vibrating sample magnetometer (VSM) as shown in the hysteresis loop presented in Figure 1b. The parallelepipedic shape grants magnetic shape anisotropy to the particles, resulting in a significant rotational torque in the rotating magnetic field, which leads to the destruction of cancer cells.

3.2. Fe-Cr-Nb-B Magnetic Nanoparticle Drug Loading. Considering that the aim of this study is to use a synergetic therapy that includes the use of magnetomechanical actuation combined with chemotherapeutic active biocompounds, we tested if Fe-Cr-Nb-B nanoparticles retain mitoxantrone and doxorubicin on their surface. Drug loading on Fe-Cr-Nb-B magnetic nanoparticle was achieved by adding a concentrated solution, i.e., 100 $\mu\text{g}/\text{mL}$ of either mitoxantrone or doxorubicin in ultrapure water further identified as MP-MTX and MP-DOX. After 24 h on a rotative shaker, nanoparticles were centrifuged, and the amount of drug adsorbed was quantified. The drug loading efficiency (DL, %) (Figure S1 in the Supporting Information) was 7.45 w/w (%) for MTX and 7.02 w/w (%) for DOX in each milligram of magnetic nanoparticles. The drug encapsulation efficiency (EE, %) in this case was 74.56% for MTX and 70.20% for DOX.

Mitoxantrone and doxorubicin used in these experiments were of pharmaceutical quality, and solutions were filtered to

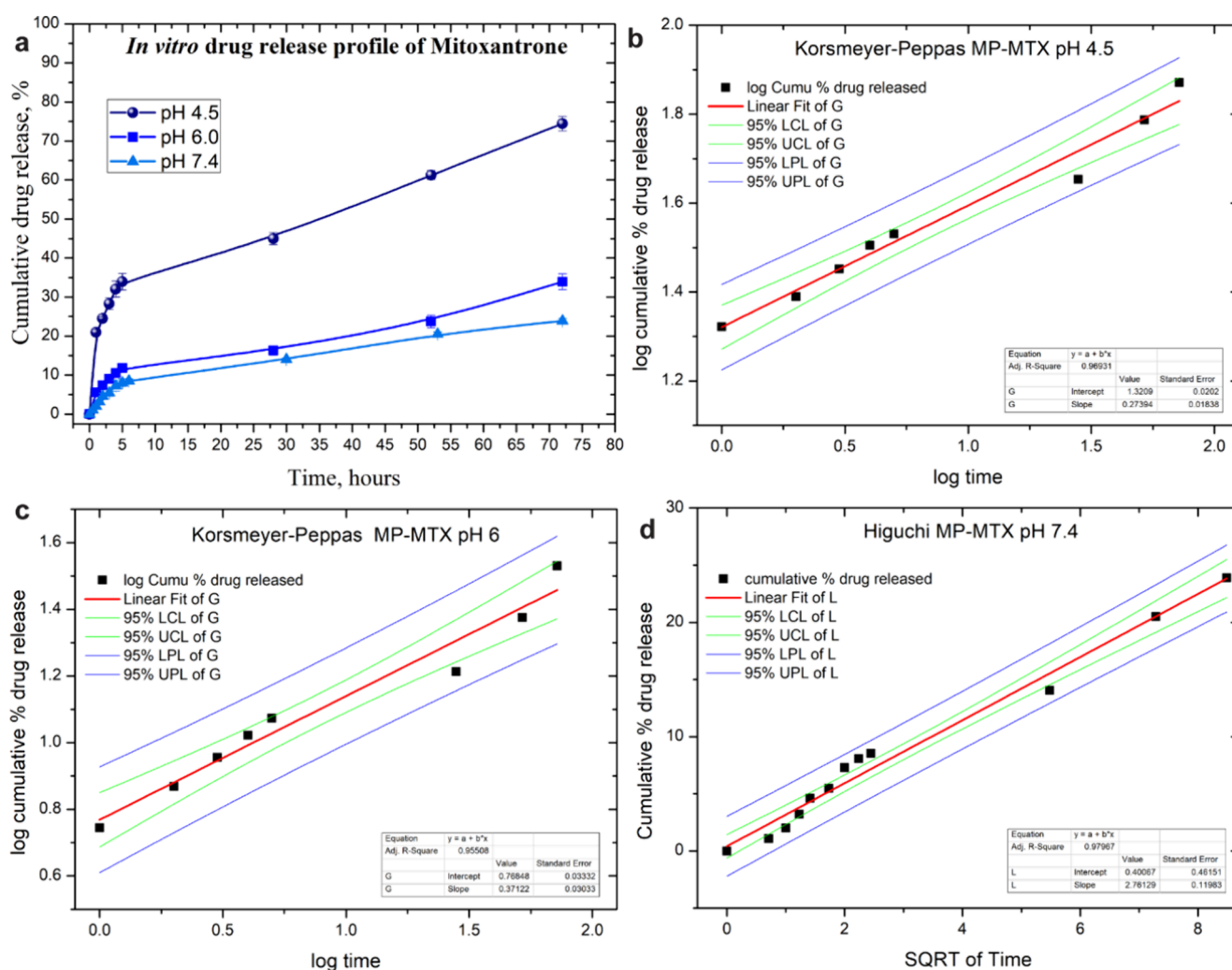


Figure 3. (a) *In vitro* drug release profile of mitoxantrone at different pH values of 4.5, 6, and 7.4. (b–d) Release kinetics of mitoxantrone from magnetic Fe-Cr-Nb-B nanoparticles at (b) pH 4.5 corresponding to the fitted Korsmeyer–Peppas model $R^2=0.969$, (c) pH 6 corresponding to the fitted Korsmeyer–Peppas model $R^2=0.955$, and (d) pH 7.4 corresponding to the fitted Higuchi model $R^2=0.979$.

be sterilized; further loading was performed under aseptic conditions in each experiment.

According to several studies,^{18–22} magnetic nanoparticles are coated and functionalized with polymers, surfactants, or proteins for the enhancement of the drug loading efficiency of antitumoral substances. The polymer coatings also may bring several disadvantages, such as possible cytotoxicity, high molecular weight with an increase of nanoparticle size, and specific surface chemistry that leads to limited drug choices and more steps in particle synthesis. The drug loading capacity of Fe-Cr-Nb-B MPs is 7.45% MTX and 7.02% DOX w/w without the functionalization of the MPs with a polymer shell. Thus, this type of nanoparticle can be used in a simplified method of adsorbing chemotherapeutic drugs on their surface in large quantities.

3.2.1. Fourier Transform Infrared Spectroscopy (FTIR) Analysis. The Fourier transform infrared (FTIR) spectroscopic analysis of Fe-Cr-Nb-B magnetic nanoparticles loaded with mitoxantrone and doxorubicin as active pharmaceutical ingredients reveals intriguing insights into the molecular interactions and chemical changes occurring at the nanoparticle–drug interface. The observed wavenumbers for pristine Fe-Cr-Nb-B magnetic nanoparticles as well for Fe-

Cr-Nb-B magnetic nanoparticles loaded with mitoxantrone (MP-MTX) and doxorubicin (MP-DOX) offer a detailed perspective on the binding modes and potential modifications within the composite system as presented in Figure 2.

The FTIR spectra of pristine Fe-Cr-Nb-B magnetic nanoparticles loaded with mitoxantrone and doxorubicin provide valuable insights into the binding modes and potential chemical changes between counterparts, enhancing our understanding of the present drug delivery system. The stretching vibrations observed in the FTIR spectrum of Fe-Cr-Nb-B magnetic nanoparticles loaded with doxorubicin provide compelling evidence of drug–molecule interactions. Bands at 3754 and 3437 cm^{-1} correspond to the free –OH and water –OH stretching vibrations, whereas the band at 3240 cm^{-1} corresponds to vibrational modes linked to the stretching vibration of N–H functional groups. Additional bands observed at 2923 and 2852 cm^{-1} were assigned to methyl –CH₃ *sym.* and *asym.* stretching vibrations present in the spectrum of DOX. Significantly, the appearance of peaks at 1628 and 1366 cm^{-1} reveals possible hydrogen bonding and complex formation between the doxorubicin active pharmaceutical ingredient and the surface of the Fe-Cr-Nb-B magnetic nanoparticles, signifying a robust association. Vibration bands

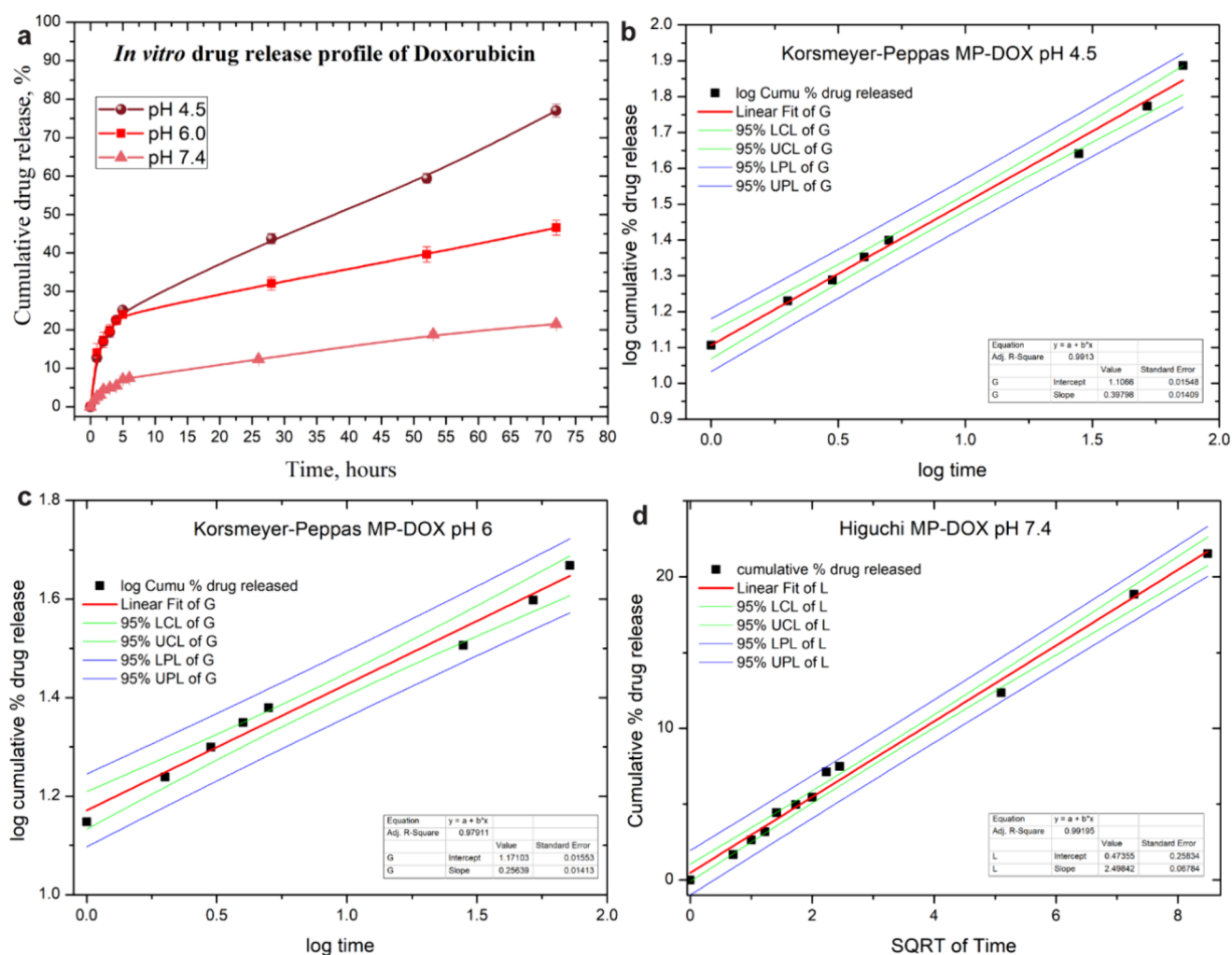


Figure 4. (a) *In vitro* drug release profile of doxorubicin at different pH values of 4.5, 6, and 7.4. (b–d) Release kinetics of doxorubicin from magnetic Fe-Cr-Nb-B nanoparticles at (b) pH 4.5 corresponding to the fitted Korsmeier–Peppas model $R^2=0.991$, (c) pH 6 corresponding to the fitted Korsmeier–Peppas model $R^2=0.979$, and (d) pH 7.4 corresponding to the fitted Higuchi model $R^2=0.991$.

located at 1290 and 1081 cm^{-1} further confirm the presence of the drug on the nanoparticle's surface, potentially inducing modifications within the local chemical environment. Similarly, the FTIR spectrum of Fe-Cr-Nb-B magnetic nanoparticles loaded with mitoxantrone reveals characteristic peaks at 3758, 3437, and 3239 cm^{-1} , confirming interactions between the surface of Fe-Cr-Nb-B magnetic nanoparticles and the mitoxantrone functional groups. The presence of absorption bands at 2927, 2847, 1632, 1394, 1186, and 1080 cm^{-1} indicates similar interactions as described for doxorubicin. Moreover, the lack of discernible vibration bands in the FTIR spectra of pristine Fe-Cr-Nb-B magnetic nanoparticles underscores their amorphous nature in the alloy form. This intrinsic absence of well-defined vibrational modes serves as a foundational reference, enabling a clear differentiation and understanding of the unique interactions observed upon loading with doxorubicin or mitoxantrone. Specifically, in both cases, namely, MP-MTX and MP-DOX systems, the FTIR spectra reveal the presence of vibration bands under the 700 cm^{-1} region, especially at 680, 593, and 479 cm^{-1} for doxorubicin-loaded nanoparticles and at 676, 588, and 498 cm^{-1} for mitoxantrone-loaded nanoparticles. These distinct features present in the MP-MTX and MP-DOX systems suggest a noteworthy phenomenon such as a partial surface

oxidation of the Fe-Cr-Nb-B magnetic nanoparticles upon loading with the active pharmaceutical ingredients (considering the wet experimental conditions applied). The presence of these bands can be attributed to metal–oxygen (Me–O) stretching vibrations, indicating changes in the oxidation state of the metallic constituents within the Fe-Cr-Nb-B magnetic nanoparticles composition. This surface oxidative phenomenon underscores the complex interplay between the loaded drugs mitoxantrone and doxorubicin and the nanoparticle matrix, potentially involving redox reactions or alterations in the local chemical environment. Furthermore, the partial surface oxidation could be linked to the interaction between the mitoxantrone and doxorubicin drug molecules and the Fe-Cr-Nb-B magnetic nanoparticles surface, potentially influencing the positive reactivity of the Fe-Cr-Nb-B MPs. The *vide supra* mentioned oxidative phenomenon might also be connected to the good release mechanisms of mitoxantrone and doxorubicin, impacting their therapeutic efficacy and stability. The identification of metal–oxygen stretching vibrations not only emphasizes the dynamic nature of the nanoparticle–drug interaction but also suggests avenues for further investigation into the mechanistic intricacies governing the composite system.

Table 1. *In Vitro* Release Kinetics of Mitoxantrone and Doxorubicin from Fe-Cr-Nb-B Nanoparticles at Various pH Values

sample	kinetic models									
	zero order ^a		first order ^b		Korsmeyer–Peppas ^c		Higuchi ^d		Hixson–Crowell ^e	
	R ²	K ₀	R ²	K	R ²	K	R ²	K _H	R ²	k
MP-MTX pH 4.5	0.818	0.766	0.927	0.015	0.969	0.273	0.922	7.17	0.902	0.018
MP-MTX pH 6.0	0.906	0.370	0.923	0.004	0.955	0.371	0.940	3.35	0.918	0.006
MP-MTX pH 7.4	0.894	0.310	0.916	0.003	0.925	0.562	0.979	2.76	0.909	0.005
MP-DOX pH 4.5	0.928	0.895	0.964	0.017	0.991	0.397	0.983	8.16	0.963	0.021
MP-DOX pH 6.0	0.754	0.465	0.840	0.006	0.979	0.256	0.896	4.46	0.813	0.009
MP-DOX pH 7.4	0.906	0.280	0.925	0.003	0.982	0.491	0.991	2.49	0.918	0.004

$${}^a Q_t = Q_0 + K_0 t. \quad {}^b \log C = \log C_0 - \frac{Kt}{2.303}. \quad {}^c \frac{M_t}{M_{\infty}} = Kt^n. \quad {}^d f = K_H \sqrt{t}. \quad {}^e \sqrt[3]{Q_t} = \sqrt[3]{Q_0} + kt.$$

3.3. *In Vitro* Drug Release Profile of MTX or DOX from Fe-Cr-Nb-B Particles. Release profiles of mitoxantrone and doxorubicin from MPs were evaluated for testing the quantity of drug that was delivered upon reaching cancer areas and surrounding healthy tissues. Both MP-MTX and MP-DOX particles were dialyzed against the culture medium without phenol red (to minimize interference in absorbance reading) at pH 7.4, 6, and 4.5. The pH of 7.4 was selected to simulate the body's physiological conditions, also paired with cell culture conditions where further experiments would take place. The pH of 6 mimics the pH inside endosomes and also the slightly acidic environment of tumor cells. The pH of 4.5 is similar to the pH of the lysosome compartment, where the magnetic particles are transported by endosomes and end up for degradation purpose. Figures 3a and 4a show the cumulative release curves of both MTX and DOX for 72 h.

A major problem in administering chemotherapeutic drugs is the spread of the substances in all systemic circulation, affecting both healthy and tumor areas.²³ For MPs presented here, at pH of 7.4, after 24 h, only 12.5% of the MTX and 12% of the DOX were released, with more than 85% of drugs remaining encapsulated, suggesting that in the case of bloodstream transportation or injection near the tumor area, drug-loaded MPs will release only a limited amount of drug in healthy areas. Also, when using ADSCs loaded with MP-(MTX/DOX) as nanoparticle carriers, released drugs would not significantly affect carrier cells. After 72 h, the amount of released MTX and DOX was 24 and 21.5%, respectively.

At pH 6, there was an increase in the drug release of both MTX and DOX. MTX release after 72 h was almost 34%, with 12% of total encapsulated drug released in the first 5 h. DOX value was almost 47% after 72 h and 23% in the first 5 h.

At pH of 4.5, the most acidic environment, drug release was consistently higher, reaching 74% for MTX and 77% for DOX. The acidic pH facilitates the release of the drug compound from the particle surface, meaning that once the particle reaches the tumor acidic microenvironment²⁴ or endosome/lysosome²⁵ compartment, the quantity of chemotherapeutic drug release should be higher compared to nonacidic pH in normal cells.

A complete release profile was not seen after 72 h for both MTX and DOX, as further nanoparticle transporting and MMA experiments take place in an interval of 72 h after which drug-loaded nanoparticles would end up inside HOS cells, overcoming tumor drug resistance.

The comprehensive analysis of drug release from magnetic Fe-Cr-Nb-B nanoparticles loaded with mitoxantrone or doxorubicin plays a pivotal role in understanding the process of delivering active pharmaceutical ingredients in a controlled

manner. Accordingly, we have employed a series of five kinetic models (Table 1), including the zero-order, first-order, Korsmeyer–Peppas, Higuchi, and Hixson–Crowell models, to elucidate the release mechanisms of mitoxantrone (Figure 3 and Figure S2–S4 in the Supporting Information) and doxorubicin (Figure 4 and Figures S5–S7 in the Supporting Information) from magnetic nanoparticles-based systems under various pH conditions such as 4.5, 6, and 7.4. Figure 3 shows the *in vitro* drug release profile of mitoxantrone and the corresponding best mathematical fitted release kinetic models from magnetic Fe-Cr-Nb-B nanoparticles at different pH values (4.5, 6, and 7.4). The release profiles exhibit distinct patterns influenced by the pH values; at acidic pH 4.5 and 6, MTX release follows a controlled mechanism, as indicated by the high goodness of fit ($R^2 = 0.969$ and 0.955) to the Korsmeyer–Peppas model, the release behavior being predominantly governed by diffusion processes. Conversely, at a higher pH value of 7.4, the release kinetics of MTX from the nanoparticles fits well ($R^2 = 0.979$) to the Higuchi model, suggesting a diffusion-controlled mechanism for drug release. The presented results are consistent with expectations for systems where drug diffusion is the primary mode of release, and it highlights the pH-dependent behavior of the magnetic Fe-Cr-Nb-B nanoparticles in releasing MTX.

A similar behavior is encountered in Figure 4, which illustrates the *in vitro* drug release profile of doxorubicin at varying pH values (4.5, 6, and 7.4) along with the corresponding best mathematical fitted release kinetics models. At pH 4.5 and 6, the release kinetics of DOX from the nanoparticles closely resembles that of mitoxantrone at the same pH (Figure 3), fitting well the Korsmeyer–Peppas model with high R^2 values of 0.991 and 0.979. The observed consistency suggests that the magnetic Fe-Cr-Nb-B nanoparticles exhibit a reliable and predictable release mechanism for different drug payloads under acidic conditions, emphasizing their potential as versatile drug delivery carriers. Moreover, at pH 7.4, similar to the observations for MTX, the release kinetics of DOX from the nanoparticles demonstrates a good fit to the Higuchi model with an R^2 value of 0.991. This reaffirms the importance of diffusion-controlled mechanisms in drug release from the magnetic nanoparticles, particularly in a biologically relevant environment.

Table 1 depicts the *in vitro* release behavior as evaluated by different kinetic models, revealing notable differences under different pH conditions and across the applied kinetic models.

Overall, the comprehensive analysis of release kinetics (Figures 3 and 4) provides valuable insights into the behavior of MTX and DOX loaded on magnetic Fe-Cr-Nb-B nanoparticles, which can lead to the design and optimization of

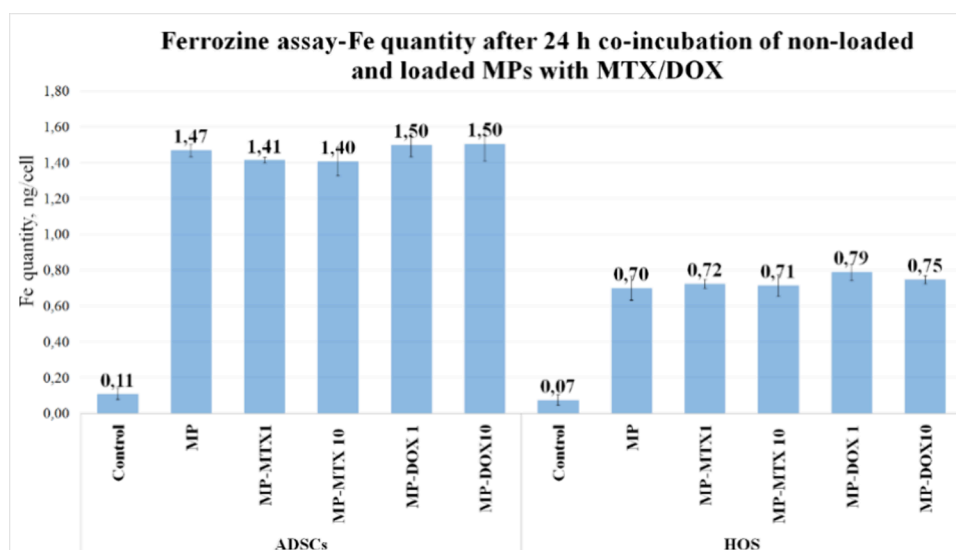


Figure 5. Ferrozine assay using spectrophotometric reading displays the iron quantity after 24 h of coincubation of ADSCs and HOS with MPs normalized to cell number. All data presented as the mean \pm SD, $n = 3$.

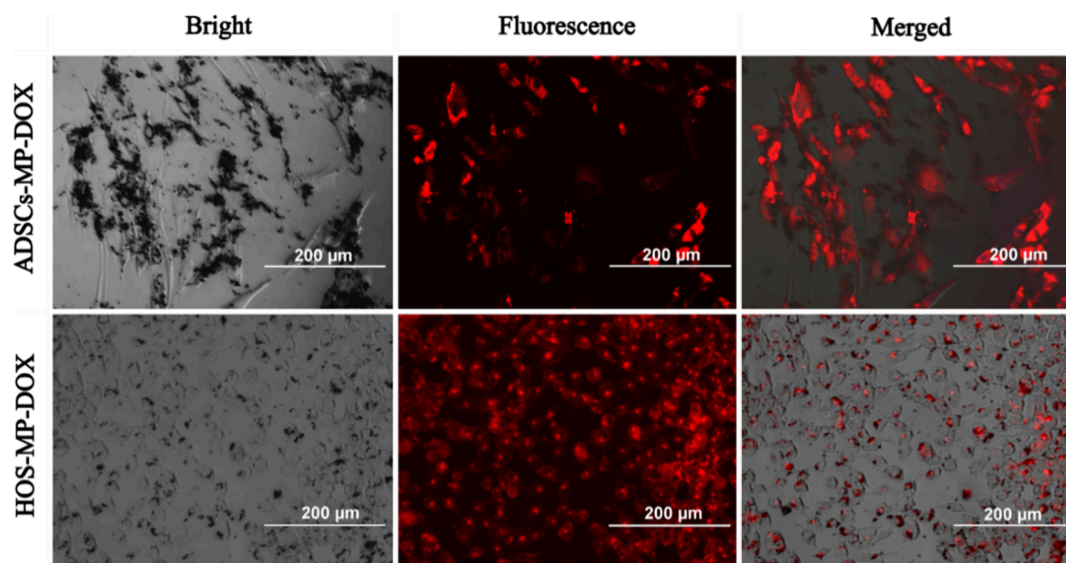


Figure 6. Cellular uptake of MP-DOX in ADSCs and HOS (bright field, fluorescence RFP filter, and merged images), scale bar = 200 μ m, EVOS inverted light microscope, 20 \times magnification.

nanoparticle-based drug delivery systems for targeted and controlled drug release applications.

3.4. Internalization of Drug-Loaded Nanoparticles.

The cellular uptake of nanomaterials is represented by several mechanisms such as endocytosis, phagocytosis, micropinocytosis, direct diffusion, and adhesive interactions.²⁶

Our recent studies⁶ showed that a concentration of 1 mg/mL of magnetic nanoparticles provided to cells was the most effective for magnetomechanical actuation. Considering the high amount of drug for both MTX and DOX of 7% w/w adsorbed on MPs, it was decided to reduce the dose of chemotherapeutic compound to 1 and 10 μ g for each milligram of MPs. The purpose is to use a dose as low as possible due to the side effects of antitumor drugs given that these affect both the healthy and cancer cells. For the following experiments, we selected to deliver a sufficient concentration of MTX or DOX that would lower cancer cell viability while maintaining a relative nontoxic dose for healthy cells. Thus, the

magnetic nanoparticles were drug-loaded with MTX/DOX at concentrations of 1 μ g/1 mg of MPs, i.e., MP-MTX1 and MP-DOX1, and at concentrations of 10 μ g/1 mg of MPs, i.e., MP-MTX10 and MP-DOX10.

To determine if Fe-Cr-Nb-B nanoparticles (drug-loaded and nonloaded) enter the cellular body, a ferrozine assay was performed. The ferrozine assay identifies the Fe compound found in Fe-Cr-Nb-B nanoparticles and quantifies the amount of nanoparticles located in the cell and on the surface of the cell membrane through adhesive interactions. The ferrozine assay was carried out in 24-well plates, testing the following batches of particles: MP, MP-MTX1, MP-MTX10, MP-DOX1, and MP-DOX10. Both cell lines, ADSCs and HOS, were used for testing the uptake of the nanoparticles. The total amount of Fe was normalized to the number of cells, so the obtained results, shown in Figure 5, indicate the quantity of magnetic nanoparticles per cell.

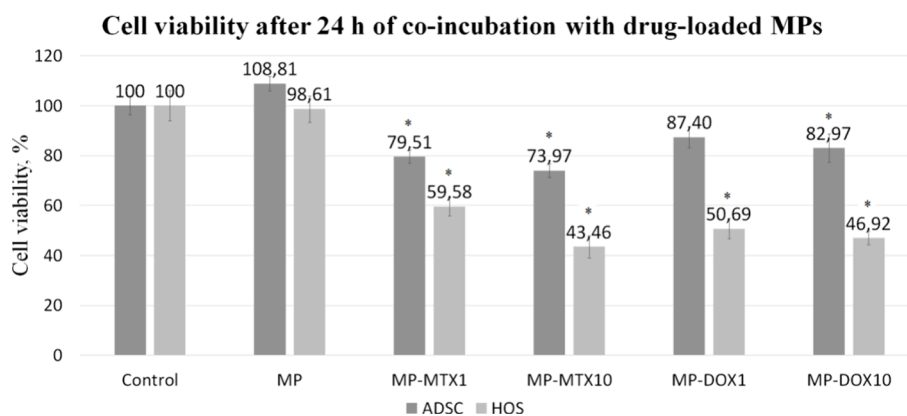


Figure 7. MTT assay indicating cell viability of ADSCs and HOS after 24 h of co-incubation with nonloaded and drug-loaded MPs (all data presented as the mean \pm SD, $n = 3$; *significantly different group relative to each control determined by one-way ANOVA at $p < 0.05$).

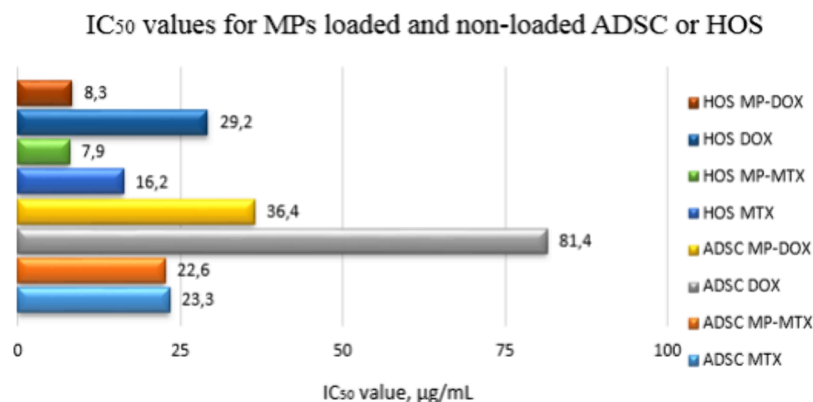


Figure 8. IC₅₀ values for ADSC-MTX/DOX and HOS-MTX/DOX versus ADSC MP-MTX/MP-DOX and HOS MP-MTX/DOX.

It is important to mention that each cell contains a normal amount of Fe used in metabolic activities; control ADSCs and HOS also contain a small quantity of Fe. After 24 h of co-incubation with nanoparticles, all samples have an increased amount of Fe compared with control, confirming nanoparticle internalization in cells, and remain attached to the cell membrane even after thorough washing. Because of the larger size of ADSCs, these cells incorporate two times more nanoparticles compared to HOS (Figure 5). Also, on account of these results, ADSCs can be considered a suitable carrier for nanoparticles toward the cancer areas. The ferrozine assay reveals that drug-loaded and nonloaded nanoparticles have the same rate of internalization in cells, with slightly increased quantity at DOX-coated nanoparticles.

Cellular uptake was also assessed using an EVOS fluorescence microscope. Doxorubicin has an intrinsic fluorescence²⁷ and can be used as a way to monitor drug-loaded nanoparticles. As can be seen in Figure 6 and Figure S8 in the Supporting Information, ADSCs and HOS were imaged after being in contact with MPs and MP-DOX. Images of bright field, fluorescence microscopy, and merged captions are presented. MPs have no intrinsic fluorescence; however, drug-loaded nanoparticles show red fluorescence, revealing nanoparticle distribution inside and onto the cellular body.

3.5. Drug-Loaded Fe-Cr-Nb-B Nanoparticle Cytotoxicity. As a first step for optimizing the delivery of MPs, drug-loaded nanoparticles were tested for cytotoxicity effect. Each type of MPs loaded and nonloaded (1 mg/mL) was added over a confluent ADSC and HOS cell culture in 96-well plates

with cell culture medium. After 24 h of interaction, cell viability was evaluated by the MTT assay. Simultaneously, several concentrations of MTX and DOX were tested to determine cell viability and IC₅₀ value (Figure S9 and S10 in the Supporting Information). Tests were performed by adding a solution of MTX/DOX in cell culture media, which were co-incubated for 24 h and assessed by the MTT assay.

As shown in Figure 7, magnetic nanoparticles do not affect the ADSCs or HOS. Fe-Cr-Nb-B particles are internalized by cells by endocytosis as the majority of nanoparticles under 200 nm²⁸ and the formed vesicles (endosomes) are transported to the lysosomal compartment where acidic environment facilitates the dissolving and deliverance of Fe ions from MPs which are further employed in cell activity and iron storage.²⁹ Cell viability with MPs is similar to ADSCs and HOS control, denoting that MPs alone do not have a cytotoxic effect on normal/cancerous cell lines and further demonstrating the potential of Fe-Cr-Nb-B particles as biocompatible drug carriers.

Cells were also exposed to MP-MTX at 1 and 10 µg/mg of nanoparticles, and a similar procedure was done for DOX-loaded MPs. As can be seen in Figure 7, MP-MTX10 and MP-DOX10 decreased the cell viability for HOS culture to as low as 43% for MP-MTX and 46% for MP-DOX. At the same time, the ADSC cell culture presents increased viability compared to HOS after drug-loaded nanoparticles exposure, reducing it slightly in DOX samples by 12–18% and in MTX samples by 21–26%. These results indicate that drug-loaded Fe-Cr-Nb-B nanoparticles are effective in decreasing HOS viability while

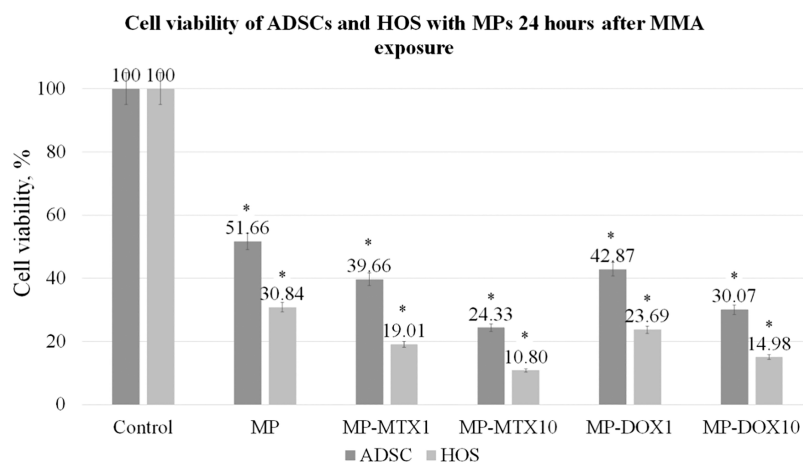


Figure 9. MTT assay 24 h following MMA exposure of ADSCs and HOS with MP, MP-MTX, and MP-DOX (all data presented as the mean \pm SD, $n = 3$, *significant difference compared to each control confirmed by one-way ANOVA, $p < 0.05$).

maintaining a relatively noncytotoxic effect on normal ADSC cell line after 24 h of incubation time. A potential cause of the cytotoxic effect could be the difference between the metabolic activities of tumoral and normal cell lines. As is known, cancer cells have an enhanced metabolism needed for sustaining rapid growth and division.³⁰ As a result of heightened metabolic uptake, a higher quantity of chemotherapeutic drugs enters the cell body and considerably affects the tumor cell population.

Also, the IC_{50} value for pure drugs was found to be 81.4 $\mu\text{g}/\text{mL}$ for ADSC-DOX, 23.3 $\mu\text{g}/\text{mL}$ for ADSC-MTX, 29.2 $\mu\text{g}/\text{mL}$ for HOS-DOX, and 16.2 $\mu\text{g}/\text{mL}$ for HOS-MTX, whereas IC_{50} for drug loaded nanoparticles was found to be 36.4 $\mu\text{g}/\text{mL}$ for ADSC-MP-DOX, 22.6 $\mu\text{g}/\text{mL}$ for ADSC-MTX, 8.3 $\mu\text{g}/\text{mL}$ for HOS-DOX, and 7.9 $\mu\text{g}/\text{mL}$ for HOS-MTX. The results presented in Figure 8 suggest a significant decrease in the concentration of drugs required to induce 50% cell mortality when loaded onto nanoparticles. Consequently, the results indicate the potential of nanoparticle-based drug delivery systems to achieve therapeutic efficacy with reduced drug dosages, thereby potentially minimizing the associated side effects.

The doxorubicin and mitoxantrone mechanism of action involves the ability to intercalate in the DNA helix and may cause its cross-linking and strand breakage, leading to inhibition of DNA and RNA synthesis.^{31,32} After ADSCs and HOS were treated with MP-MTX and MP-DOX, several nucleic changes could be observed using fluorescence microscopy. Cells were stained with DAPI staining to highlight the cell nuclei. Figure S11 in the Supporting Information underlines that cells treated with MPs maintain the same nucleus structure as control cells; however, drug-loaded MP counterparts display a heavily modified structure. The image of ADSCs and HOS with drug-loaded MPs presents morphological changes like crescent shape, fragmentation, varying size and shape nuclei, pyknosis, and condensed chromatin, which suggest apoptotic cells; also, some nuclei show nuclear DNA leakage, particularly in HOS cells.

3.6. Magnetomechanical Actuation of Drug-Loaded Nanoparticles Inside ADSC and HOS Cell Cultures.

3.6.1. Viability of ADSCs and HOS after Magnetomechanical Actuation of Drug-Loaded MPs. The synergistic therapy proposed here has a drug-related mechanism that was presented above and a magnetomechanical mechanism complementary to the already drug-affected cells. Magneto-

mechanical actuation takes place in a four-coil system that generates a uniform magnetic field inside the system area. The 96-well plates with HOS and ADSCs were placed inside the self-made system and were actuated in a rotating magnetic field. Preliminary to tests, cells at 90% confluency were incubated with 1 mg/mL of nonloaded and drug-loaded nanoparticles for 24 h to allow nanoparticle internalization. The MMA session lasted 30 min. Fe-Cr-Nb-B nanoparticles inside the MMA device gain a rotational motion, leading to movement and cell destruction. To evaluate the effect of nanoparticles under the influence of MMA on cell cultures, an MTT viability test was used.

Viability tests were performed 24 h after magnetomechanical actuation. After ADSCs and HOS were exposed to MMA, cell viability was identified with an MTT assay. As can be seen in Figure 9 compared to Figure 7, a significant increase in cell death was obtained due to magnetic field action. Samples containing only magnetic particles showed a viability of 51% for ADSCs and 30% for HOS; thus, nanoparticle loaded cells are destroyed by applying a magnetic field inducing particle movement inside or outside of the cells.

Some research papers have studied the behavior of different types of magnetic particles for medical applications, which utilize the magnetomechanical effect. These include SPION magnetite particles,³³ disc-shaped particles that have been fabricated through the combination of vacuum-deposition techniques with lithography techniques,³⁴ as well as different kinds of magnetic nanowires (NWs).³⁵

The conducted studies have demonstrated that MMA is a promising approach toward cancer cell research. These studies have highlighted the various magnetic particles that can be utilized to destroy cancer cells via MMA. The previously obtained results have emphasized the efficiency of Fe-Cr-Nb-B MPs, when magnetomechanically actuated, in targeting and destroying cancer cells.

Likewise, drug-loaded nanoparticles combined with MMA led to extremely low cell viability in both cell lines. MP-MTX samples show a viability in the range 10–19% for HOS and 24–39% for ADSCs, being inversely related to drug concentration. MP-DOX shows a viability of 30–42% for ADSCs and 14–23% for HOS. A related point to consider is that in all previously mentioned samples, ADSCs have better viability compared to similar samples for HOS, denoting that ADSCs are not as negatively influenced compared with HOS.

3.6.2. LDH (Lactate Dehydrogenase) Assay after Magnetomechanical Actuation of Drug-Loaded MPs. The LDH cytotoxicity assay identifies the quantity of cytosol leakage in the cell culture medium. The cytosolic enzyme lactate dehydrogenase (LDH) is released from cytosol in the case of irreversible cell membrane damage and is identified by a formazan reaction, which indicates the amount of dead cells compared to a maximum LDH activity control where 100% of cells are lysed by a lysis buffer.

The LDH cytotoxicity assay was performed under conditions similar to those of the MTT assay. Ninety-six-well plates with ADSC and HOS cell cultures at confluency were treated with 1 mg/mL of MPs, MP-MTX1, and MP-DOX1. After 24 h, once nanoparticles were incorporated, cells were submitted to magnetomechanical actuation for 30 min and assessed with the LDH assay after 12 h.

The LDH assay (Figure 10) confirmed that all cells subjected to MMA, particularly MPs-loaded cells, show

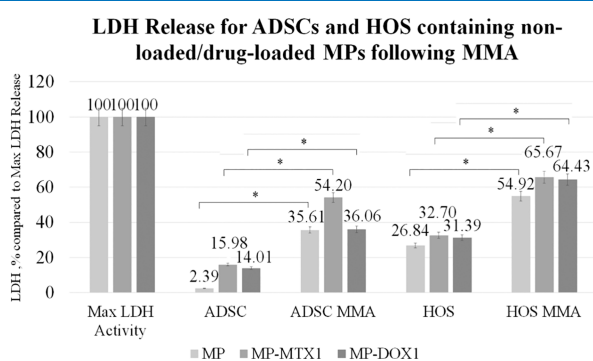


Figure 10. LDH assay displaying the percentage of ADSC and HOS cells that exhibit cytosol leakage, meaning cell death, 12 h after MMA session (all data presented as the mean \pm SD, $n = 3$, *significant difference between the MMA group versus the nonexposed group confirmed by one-way ANOVA for $p < 0.05$).

significant cell membrane damage, leading to cytosol leakage and, subsequently, cell death. The most affected cells are HOS, which elicit 55–65% cytotoxicity in MMA samples, generally higher than nonactuated samples. Magnetomechanical actuation leads to an increased cell death rate, by 20–30% in both cell lines, whereas all drug-loaded MPs samples add another 10–19% due to the MMA effect except for ADSCs-MP-DOX. The LDH assay corroborated the MTT results, supporting the assumption that magnetomechanical actuation coupled with cell internal drug release induces irreparable cell damage. This new approach of complementary therapy may enhance cancer cell therapies.

3.6.3. Live/Dead Assay of ADSCs and HOS before versus after Magnetomechanical Actuation. The live/dead assay provides a two-color method of labeling the live and dead cells with fluorescent dyes. Live cells have intracellular esterase activity and can be stained with green-fluorescent calcein-AM fixating onto the entire cell body, whereas dead cells that lost plasma integrity are stained with red-fluorescent ethidium homodimer-1 that binds on the cell nuclei.

Drug-loaded and nonloaded MPs were added to ADSC and HOS cells at 90% confluency. After 24 h, cell plates were subjected to MMA for 30 min. Live/dead fluorescence staining clearly reveals that ADSCs and HOS control cells are unaffected after exposure to the magnetic field. However, all cells containing MPs have a lower cell viability, indicated by

more dead cells (red nuclei), the lowest being drug-loaded samples. In the following images, the additional unoccupied spaces between green cells were occupied by unattached dead cells and were washed during the live/dead protocol. Figure 11 and Figure S12 in the Supporting Information indicate the MMA effect in the case of nonloaded and MP-loaded ADSCs. For ADSCs, both control and MMA control appear fusiform, with an elongated cell shape and good attachment to the cell culture dish, thus being 100% viable cells. ADSCs containing MPs show no cytotoxic effect and good viability, but the same could not be seen for the MMA counterpart. The shape of the cellular body highlights the processes inside the cytoplasm. All ADSCs that contain MPs and undergo an MMA session show signs of distress and change in cell shape as well as irregular and low attachment to cell culture dish and eventual detachment and subsequent death. The green fluorescence can also be present in apoptotic cells, live cells that are programmed to die, which have a disproportionate shape after MMA but are not yet dead.

Furthermore, HOS cells were subjected to identical treatment as their ADSC counterparts, and the live/dead assay was performed. Figure 11 and Figure S13 in the Supporting Information show the morphology of HOS cells before and after the MMA. The dimension of the HOS cell is significantly smaller compared to ADSC and subsequently encloses a lower MP quantity also confirmed by the ferrozine assay; however, it is enough for the MP targeting and injuring. HOS control cells retain cell homeostasis under the magnetic field. Nonetheless, the HOS cells enclosing MP were severely affected by magnetomechanical actuation, drug-loading, or both. The cell attachment is vastly disturbed, with cells tending to take a spherical form and lose the dish adhesion, meaning that the cell is in the apoptosis phase or deceased. The live/dead images confirm that MPs alone under MMA influence lead to cell damage but coupled with drug antitumor mechanism significantly decrease the cell viability.

3.7. Magnetomechanical Actuation of ADSCs Transporting Drug-Loaded Nanoparticles in Osteosarcoma Cell Culture. Considering the proposed antitumor treatment involving drug-loaded nanoparticles coupled with MMA, our group further tested a “Trojan Horse” strategy that consisted of delivering drug-loaded nanoparticles using ADSCs. ADSCs, as shown above in Figure 5, incorporate in their cytosol and on the membrane surface a significant amount of magnetic nanoparticles due to their increased size compared to HOS cells. ADSCs are known for tumor targeting and inhibition of certain cancer types,^{36–38} which make them a suitable candidate for carrying drug-loaded nanoparticles to tumor sites bypassing nanoparticle body clearance and allowing the delivery of the entire quantity of nanoparticles loaded in ADSCs to tumor sites. For successful delivery, we propose to magnetomechanically actuate ADSCs filled with drug-loaded nanoparticles while located at tumor sites. To encapsulate particles, ADSCs in 96-well plates were subjected to a 24 h incubation with MPs/drug-loaded MPs at a concentration of 1 mg/mL. ADSCs were thoroughly washed two times with PBS to eliminate nanoparticle excess and trypsinized. Detached cells were transferred onto a HOS cell culture at confluency. After 2 h while ADSCs were still in suspension, cells were exposed to MMA for 30 min. In the first round of MMA, ADSCs presented cell membrane rupture and released onto HOS the carried nanoparticles. After another 24 h, when released nanoparticles were incorporated by HOS, one more

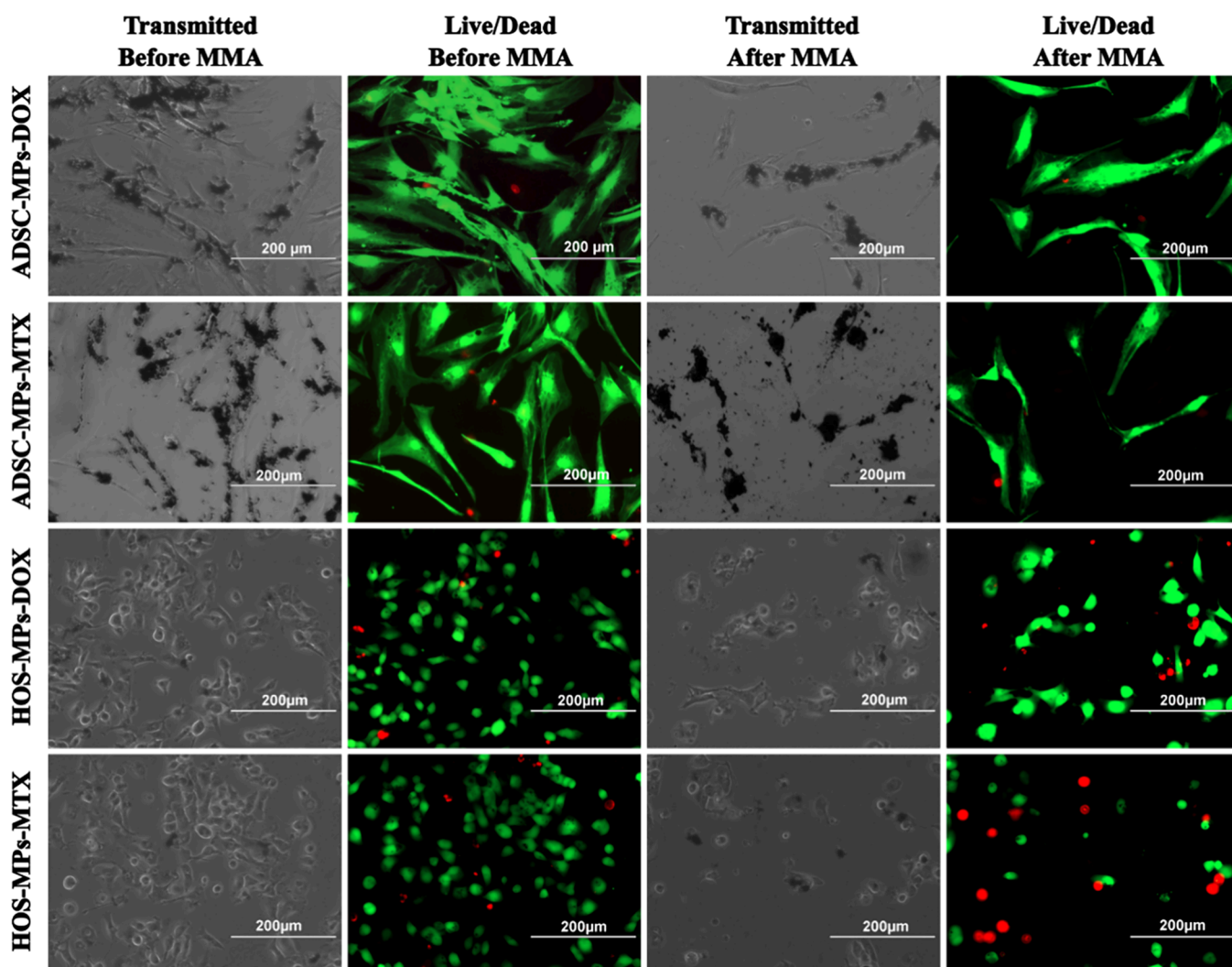


Figure 11. Live/dead assay representing ADSC and HOS before and after magnetomechanical actuation. The presented images contain ADSC-MPs-DOX, ADSC-MPs-MTX, HOS-MPs-DOX, and HOS-MPs-MTX. Images taken in transmitted light and fluorescence GFP and RFP filters. Live (GFP filter) and dead (RFP filter) images were merged to obtain live/dead images with the EVOS inverted light microscope. Magnification 20 \times . Scale bar 200 μ m.

MMA round was applied. After 24 h, MTT and LDH assays were performed.

Figure 12 shows that both MTT and LDH assays prove that a concentration as low as 1 μ g/mg of drug loaded onto MPs may reduce cell viability to 75% using only the drug component in this ADSCs–HOS coculture and even lower to 70% for a concentration of 10 μ g/mg of drug-MPs. When applying a magnetic field and using synergetic therapy, cell viability is as low as 41% for MTX samples. The most damaged samples are MTX followed by the DOX samples.

4. CONCLUSIONS

The scope of our study was to describe a new technique of using a synergistic therapy in cancer treatment using Fe-Cr-Nb-B magnetic particles. The double tactic consists of combining chemotherapeutic drugs with magnetomechanical actuation, both being delivered by the use of a single nanovehicle: the magnetic nanoparticle. The advantage of drug-loaded magnetic nanoparticles in cancer treatment is the high targeting capacity using a magnetic field, especially on near-surface localized cancers; lower toxicity; and fewer side

effects due to precise drug delivery. The MPs are prepared by mechanical grinding and present remarkable magnetic properties and high anisotropy. Fe-Cr-Nb-B magnetic nanoparticles, without coatings of either polymers or supplementary surfactants, were loaded with chemotherapeutic drugs mitoxantrone or doxorubicin in high quantities (7.45% MTX and 7.02% DOX w/w). The quantity of chemotherapeutics loaded onto MPs may be adjustable depending on the purpose, which results in increasing or reducing the drug quantity and, consequently, the drug toxicity.

The cytotoxicity of drug-loaded MPs was evaluated by the MTT assay and cell nucleus DAPI staining in both ADSCs and HOS cultures for the following chemotherapy treatment assessment. Results showed that the antitumoral drugs loaded onto MPs lead to a decrease of 43% in HOS cell viability and only 74% in ADSCs, showing that normal cells are less impacted by MTX and DOX compared to tumoral cells. The study further investigated cells that were magnetomechanically actuated, evaluating cell death through MTT and LDH assays and live/dead cell staining in both cell lines. The obtained findings suggest that MMA together with drug therapy led to another decrease of 30% in cell viability, i.e., to a viability of

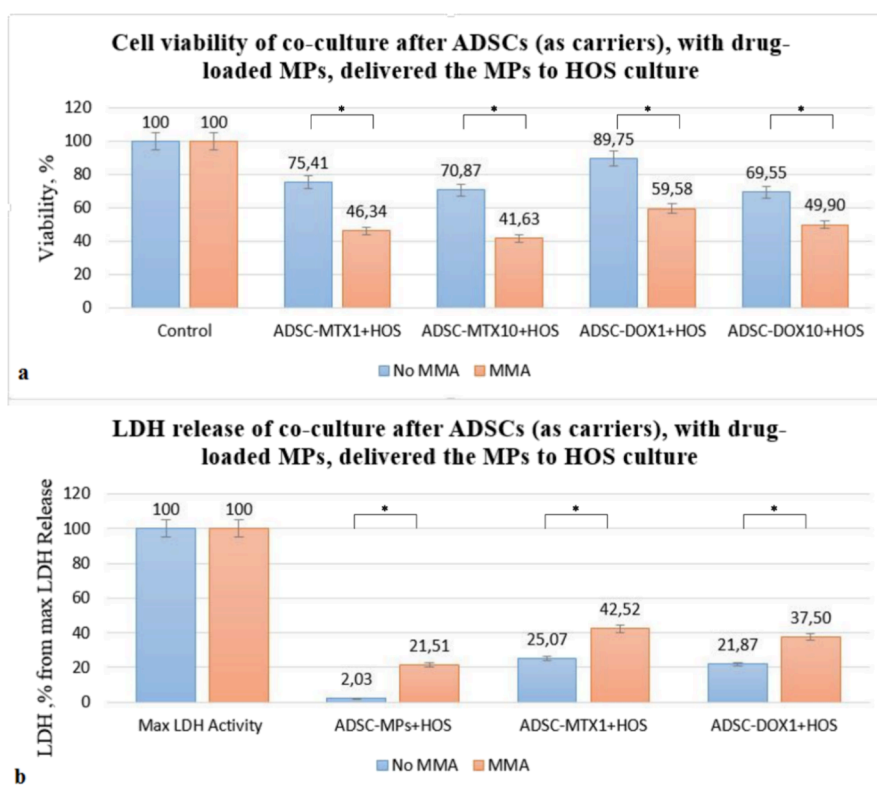


Figure 12. (a) MTT viability assay and (b) LDH cytotoxicity assay. The MMA was applied to ADSCs containing drug-loaded nanoparticles while located at tumor sites in HOS, and after 24 h, another MMA session was applied once MPs entered HOS cells (all data presented as the mean \pm SD, $n = 3$, *significant difference between the MMA group versus the nonexposed group confirmed by one-way ANOVA for $p < 0.05$).

10% for HOS and 24% for ADSCs. The combination of these drugs with magnetomechanical actuation provided a synergistic effect that significantly enhanced cancer cell destruction.

Additionally, ADSCs have shown potential in cancer therapy through nanoparticle drug delivery and tumor targeting. The drug-loaded MPs were successfully internalized by ADSCs in large quantities, two times higher than in HOS cells due to their different sizes, at the same rate as nonloaded MPs. HOS culture, receiving drug-loaded MPs carried by ADSCs, showed a significant reduction in cell viability, reaching 41% after two rounds of magnetomechanical actuation. The MMA exposure together with the chemotherapeutic drugs transported by MPs led to cell/lysosomal membrane disruptions and cell death. The nanoparticle vehicle helped to overcome drug-resistance issues, decreasing conventional high doses of drugs used in systemic administration, whereas ADSCs, used as carriers for these nanoparticles, lead magnetic targeting to cancer areas, bypassing the cellular rejection mechanisms and, at the same time, delivering large quantities of MPs and antitumoral substances to the desired locations.

■ ASSOCIATED CONTENT

Data Availability Statement

The data underlying this study are available in the published article and its Supporting Information.

SI Supporting Information

The Supporting Information is available free of charge at <https://pubs.acs.org/doi/10.1021/acsomega.4c02189>.

Drug loading efficiency (Figure S1); release kinetics of mitoxantrone (Figures S2–S4) and doxorubicin (Figures S5–S7); cellular uptake of MP-DOX (Figure S8);

determination of IC_{50} value (Figures S9 and S10); nuclei staining with fluorescent DAPI dye (Figure S11); and live/dead assay (Figures S12 and S13) (PDF)

■ AUTHOR INFORMATION

Corresponding Author

Anca Emanuela Minuti – National Institute of Research and Development for Technical Physics, Iasi 700050, Romania; orcid.org/0009-0005-4319-2545; Phone: +40754648933; Email: aminuti@phys-iasi.ro

Authors

Cristina Staviță – National Institute of Research and Development for Technical Physics, Iasi 700050, Romania; Faculty of Physics, “Alexandru Ioan Cuza” University, Iasi 700506, Romania; orcid.org/0009-0002-5719-710X

Dumitru Daniel Herea – National Institute of Research and Development for Technical Physics, Iasi 700050, Romania; orcid.org/0000-0002-8455-8380

Luminița Lăbușcă – National Institute of Research and Development for Technical Physics, Iasi 700050, Romania; orcid.org/0000-0001-9635-6893

Daniel Gherca – National Institute of Research and Development for Technical Physics, Iasi 700050, Romania

Nicoleta Lupu – National Institute of Research and Development for Technical Physics, Iasi 700050, Romania; orcid.org/0000-0003-2188-8187

Horia Chiriac – National Institute of Research and Development for Technical Physics, Iasi 700050, Romania

Complete contact information is available at:

<https://pubs.acs.org/doi/10.1021/acsomega.4c02189>

Author Contributions

H.C. was responsible for designing the study and supervising the work. C.S. conducted drug loading and release studies. A.E.M. and C.S. performed the *in vitro* cell viability studies and analyzed the results. L.L. and D.D.H. studied the association of cells with MPs and magnetomechanical actuation. D.G. was responsible for data analysis, images and text of kinetic models, interpretation of kinetic data, FTIR analysis, and drug conjugation. N.L. was in charge of characterizing the magnetic particles and contributed to the interpretation of the results. H.C., C.S., A.E.M., D.G., and N.L. collaborated on writing the manuscript. All authors read and approved the final manuscript.

Funding

Financial support from the MCID Nucleu (PN 23 11 01 01) and PFE (Contract SPFE/2022) Programmes is highly acknowledged.

Notes

The authors declare no competing financial interest.

ACKNOWLEDGMENTS

Not applicable.

ABBREVIATION

ADSCs-adipose-derived mesenchymal stem cells; **DAPI**-(4',6-diamidino-2-phenylindole) staining; **DL**-drug loading efficiency; **DLS**-dynamic light scattering; **DMEM**-Dulbecco's modified Eagle medium; **DMSO**-dimethyl sulfoxide; **DOX**-doxorubicin; **EE**-drug encapsulation efficiency; **FBS**-fetal bovine serum; **FDA**-Food and Drug Administration; **FTIR**-Fourier transform infrared spectroscopy analysis; **GFP**-green fluorescent protein filter; **HOS**-human osteosarcoma; **HR-SEM**-high-resolution scanning electron microscopy; **LDH**-lactate dehydrogenase; **MMA**-Magnetomechanical Actuation; **MPs**-magnetic particles; **MTT**-3-(4,5-dimethylthiazolyl-2)-2,5-diphenyltetrazolium bromide; **MTX**-mitoxantrone; **PBS**-phosphate-buffered saline; **RFP**-red fluorescent protein filter; **VSM**-vibrating sample magnetometer

REFERENCES

- (1) Farzin, A.; Etesami, S. A.; Quint, J.; Memic, A.; Tamayol, A. Magnetic Nanoparticles in Cancer Therapy and Diagnosis. *Adv. Healthcare Mater.* **2020**, *9* (9), 1901058.
- (2) Nikitin, A. A.; Ivanova, A. V.; Semkina, A. S.; Lazareva, P. A.; Abakumov, M. A. Magneto-Mechanical Approach in Biomedicine: Benefits, Challenges, and Future Perspectives. *International Journal of Molecular Sciences* **2022**, *23* (19), 11134.
- (3) Serantes, D.; Chantrell, R.; Gavilán, H.; Morales, M. D. P.; Chubykalo-Fesenko, O.; Baldomir, D.; Satoh, A. Anisotropic Magnetic Nanoparticles for Biomedicine: Bridging Frequency Separated AC-Field Controlled Domains of Actuation. *Phys. Chem. Chem. Phys.* **2018**, *20* (48), 30445–30454.
- (4) Zhang, E.; Kircher, M. F.; Koch, M.; Eliasson, L.; Goldberg, S. N.; Renström, E. Dynamic Magnetic Fields Remote-Control Apoptosis via Nanoparticle Rotation. *ACS Nano* **2014**, *8* (4), 3192–3201.
- (5) Naud, C.; Thébault, C.; Carrière, M.; Hou, Y.; Morel, R.; Berger, F.; Diény, B.; Joisten, H. Cancer Treatment by Magneto-Mechanical Effect of Particles, a Review. *Nanoscale Adv.* **2020**, *2* (9), 3632–3655.
- (6) Chiriac, H.; Minuti, A. E.; Stavila, C.; Herea, D.-D.; Labusca, L.; Ababei, G.; Stoian, G.; Lupu, N. Fe-Cr-Nb-B Magnetic Particles and Adipose-Derived Mesenchymal Cells Trigger Cancer Cell Apoptosis by Magneto-Mechanical Actuation. *Nanomaterials* **2023**, *13* (22), 2941.

- (7) Chu, D.-T.; Nguyen Thi Phuong, T.; Tien, N. L. B.; Tran, D. K.; Minh, L. B.; Thanh, V. V.; Gia Anh, P.; Pham, V. H.; Thi Nga, V. Adipose Tissue Stem Cells for Therapy: An Update on the Progress of Isolation, Culture, Storage, and Clinical Application. *Journal of Clinical Medicine* **2019**, *8* (7), 917.

- (8) Aloss, K.; Hamar, P. Recent Preclinical and Clinical Progress in Liposomal Doxorubicin. *Pharmaceutics* **2023**, *15* (3), 893.

- (9) Goryacheva, O. A.; Pidenko, P. S.; Markin, A. V.; Markina, N. E.; Tsyupka, D. V.; Mordovina, E. A.; Ponomaryova, T. D.; Meshcheryakova, S. A.; Kornilov, D. A.; Strokin, P. D.; Drozd, D. D.; Podkolodnaya, Y. A.; Kovyrshina, A. A.; Morozova, I. V.; Shelekhova, T. V.; Goryacheva, I. Y. Current Trends and Challenges in the Mitoxantrone Measuring in Biofluids and New Pharmaceutical Systems. *TrAC Trends in Analytical Chemistry* **2023**, *169*, No. 117373.

- (10) Chiriac, H.; Lupu, N.; Lostun, M.; Ababei, G.; Grigoras, M.; Dănceanu, C. Low TC Fe-Cr-Nb-B Glassy Submicron Powders for Hyperthermia Applications. *J. Appl. Phys.* **2014**, *115* (17), 17B520.

- (11) Minuti, A. E.; Stoian, G.; Herea, D.-D.; Radu, E.; Lupu, N.; Chiriac, H. Fe-Cr-Nb-B Ferrofluid for Biomedical Applications. *Nanomaterials* **2022**, *12* (9), 1488.

- (12) Darwish, W.; Lafta, R.; Shafaa, M.; El-Nagdy, M. Mitoxantrone in Synergism with Gold Hexagonal Nanoparticles and Gamma Radiation for Effective Treatment of MCF7 Cells. *Egypt. J. Chem.* **2021**, *0* (0), 0–0.

- (13) Herea, D.-D.; Labusca, L.; Radu, E.; Chiriac, H.; Grigoras, M.; Panzaru, O. D.; Lupu, N. Human Adipose-Derived Stem Cells Loaded with Drug-Coated Magnetic Nanoparticles for in-Vitro Tumor Cells Targeting. *Materials Science and Engineering: C* **2019**, *94*, 666–676.

- (14) Dash, S.; Murthy, P. N.; Nath, L.; Chowdhury, P. Kinetic Modeling on Drug Release from Controlled Drug Delivery Systems. *Acta Polym. Pharm.* **2010**, *67* (3), 217–223.

- (15) Morgan, D. M. Tetrazolium (MTT) Assay for Cellular Viability and Activity. *Methods Mol. Biol.* **1998**, *79*, 179–183.

- (16) Riemer, J.; Hoepken, H. H.; Czerwinska, H.; Robinson, S. R.; Dringen, R. Colorimetric Ferrozine-Based Assay for the Quantitation of Iron in Cultured Cells. *Anal. Biochem.* **2004**, *331* (2), 370–375.

- (17) Chiriac, H.; Radu, E.; Țibu, M.; Stoian, G.; Ababei, G.; Lăbușcă, L.; Herea, D.-D.; Lupu, N. Fe-Cr-Nb-B Ferromagnetic Particles with Shape Anisotropy for Cancer Cell Destruction by Magneto-Mechanical Actuation. *Sci. Rep.* **2018**, *8* (1), 11538.

- (18) Comanescu, C. Magnetic Nanoparticles: Current Advances in Nanomedicine Drug Delivery and MRI. *Chemistry* **2022**, *4* (3), 872–930.

- (19) Dinter, J.; Friedrich, R. P.; Yang, H.; Pilarsky, C.; Mangge, H.; Pöttler, M.; Janko, C.; Alexiou, C.; Lyer, S. Mitoxantrone and Mitoxantrone-Loaded Iron Oxide Nanoparticles Induce Cell Death in Human Pancreatic Ductal Adenocarcinoma Cell Spheroids. *Materials* **2023**, *16* (7), 2906.

- (20) Patra, J. K.; Das, G.; Fraceto, L. F.; Campos, E. V. R.; Rodriguez-Torres, M. del P.; Acosta-Torres, L. S.; Diaz-Torres, L. A.; Grillo, R.; Swamy, M. K.; Sharma, S.; Habtemariam, S.; Shin, H.-S. Nano Based Drug Delivery Systems: Recent Developments and Future Prospects. *J. Nanobiotechnol.* **2018**, *16* (1), 71.

- (21) Pusta, A.; Tertis, M.; Crăciunescu, I.; Turcu, R.; Mirel, S.; Cristea, C. Recent Advances in the Development of Drug Delivery Applications of Magnetic Nanomaterials. *Pharmaceutics* **2023**, *15* (7), 1872.

- (22) Ratschker, T.; Egenberger, L.; Alev, M.; Zschesche, L.; Band, J.; Schreiber, E.; Frey, B.; Derer, A.; Alexiou, C.; Janko, C. Mitoxantrone-Loaded Nanoparticles for Magnetically Controlled Tumor Therapy—Induction of Tumor Cell Death, Release of Danger Signals and Activation of Immune Cells. *Pharmaceutics* **2020**, *12* (10), 923.

- (23) Anand, U.; Dey, A.; Chandel, A. K. S.; Sanyal, R.; Mishra, A.; Pandey, D. K.; De Falco, V.; Upadhyay, A.; Kandimalla, R.; Chaudhary, A.; Dhanjal, J. K.; Dewanjee, S.; Vallamkondu, J.; Pérez de la Lastra, J. M. Cancer Chemotherapy and beyond: Current Status, Drug Candidates, Associated Risks and Progress in Targeted Therapeutics. *Genes & Diseases* **2023**, *10* (4), 1367–1401.

- (24) Boedtker, E.; Pedersen, S. F. The Acidic Tumor Microenvironment as a Driver of Cancer. *Annu. Rev. Physiol.* **2020**, *82* (2020), 103–126.
- (25) Sun, Y.; Sha, Y.; Cui, G.; Meng, F.; Zhong, Z. Lysosomal-Mediated Drug Release and Activation for Cancer Therapy and Immunotherapy. *Adv. Drug Delivery Rev.* **2023**, *192*, No. 114624.
- (26) Wu, M.; Guo, H.; Liu, L.; Liu, Y.; Xie, L. Size-Dependent Cellular Uptake and Localization Profiles of Silver Nanoparticles. *IJN* **2019**, *14*, 4247–4259. *Volume*
- (27) Shah, S.; Chandra, A.; Kaur, A.; Sabnis, N.; Lacko, A.; Gryczynski, Z.; Fudala, R.; Gryczynski, I. Fluorescence Properties of Doxorubicin in PBS Buffer and PVA Films. *Journal of Photochemistry and Photobiology B: Biology* **2017**, *170*, 65–69.
- (28) Wang, T.; Wang, L.; Li, X.; Hu, X.; Han, Y.; Luo, Y.; Wang, Z.; Li, Q.; Aldalbahi, A.; Wang, L.; Song, S.; Fan, C.; Zhao, Y.; Wang, M.; Chen, N. Size-Dependent Regulation of Intracellular Trafficking of Polystyrene Nanoparticle-Based Drug-Delivery Systems. *ACS Appl. Mater. Interfaces* **2017**, *9* (22), 18619–18625.
- (29) Yaremko, A. V.; Zelepukin, I. V.; Ivanov, I. N.; Melikov, R. O.; Pechnikova, N. A.; Dzhililova, D. Sh.; Mirkasymov, A. B.; Bragina, V. A.; Nikitin, M. P.; Deyev, S. M.; Nikitin, P. I. Influence of Magnetic Nanoparticle Biotransformation on Contrasting Efficiency and Iron Metabolism. *J. Nanobiotechnol* **2022**, *20* (1), 535.
- (30) Schiliro, C.; Firestein, B. L. Mechanisms of Metabolic Reprogramming in Cancer Cells Supporting Enhanced Growth and Proliferation. *Cells* **2021**, *10* (5), 1056.
- (31) Park, S.; Lee, J.; Kang, M.; Jang, K.; Kim, J. Mitoxantrone Induces Apoptosis in Osteosarcoma Cells through Regulation of the Akt/FOXO3 Pathway. *Oncol Lett.* **2018**, DOI: 10.3892/ol.2018.8547.
- (32) Sritharan, S.; Sivalingam, N. A Comprehensive Review on Time-Tested Anticancer Drug Doxorubicin. *Life Sciences* **2021**, *278*, No. 119527.
- (33) Cheng, D.; Li, X.; Zhang, G.; Shi, H. Morphological Effect of Oscillating Magnetic Nanoparticles in Killing Tumor Cells. *Nanoscale Res. Lett.* **2014**, *9* (1), 195.
- (34) Kim, D.-H.; Rozhkova, E. A.; Ulasov, I. V.; Bader, S. D.; Rajh, T.; Lesniak, M. S.; Novosad, V. Biofunctionalized Magnetic-Vortex Microdiscs for Targeted Cancer-Cell Destruction. *Nat. Mater.* **2010**, *9* (2), 165–171.
- (35) Contreras, M. F.; Sougrat, R.; Zaher, A.; Ravasi, T.; Kosel, J. Non-Chemotoxic Induction of Cancer Cell Death Using Magnetic Nanowires. *Int. J. Nanomedicine* **2015**, *10*, 2141–2153.
- (36) Grisendi, G.; Bussolari, R.; Cafarelli, L.; Petak, I.; Rasini, V.; Veronesi, E.; De Santis, G.; Spano, C.; Tagliazzucchi, M.; Barti-Juhasz, H.; Scarabelli, L.; Bambi, F.; Frassoldati, A.; Rossi, G.; Casali, C.; Morandi, U.; Horwitz, E. M.; Paolucci, P.; Conte, P.; Dominici, M. Adipose-Derived Mesenchymal Stem Cells as Stable Source of Tumor Necrosis Factor-Related Apoptosis-Inducing Ligand Delivery for Cancer Therapy. *Cancer Res.* **2010**, *70* (9), 3718–3729.
- (37) Li, T.; Zhou, X.; Wang, J.; Liu, Z.; Han, S.; Wan, L.; Sun, X.; Chen, H. Adipose-Derived Mesenchymal Stem Cells and Extracellular Vesicles Confer Antitumor Activity in Preclinical Treatment of Breast Cancer. *Pharmacol. Res.* **2020**, *157*, No. 104843.
- (38) Xie, H.; Liao, N.; Lan, F.; Cai, Z.; Liu, X.; Liu, J. 3D-Cultured Adipose Tissue-Derived Stem Cells Inhibit Liver Cancer Cell Migration and Invasion through Suppressing Epithelial-Mesenchymal Transition. *Int. J. Mol. Med.* **2017**, DOI: 10.3892/ijmm.2017.3336.